Electronic Supplementary Material (ESI) for Lab on a Chip
This journal is © The Royal Society of Chemistry 2011

Supplementary Information

Supplementary Figures

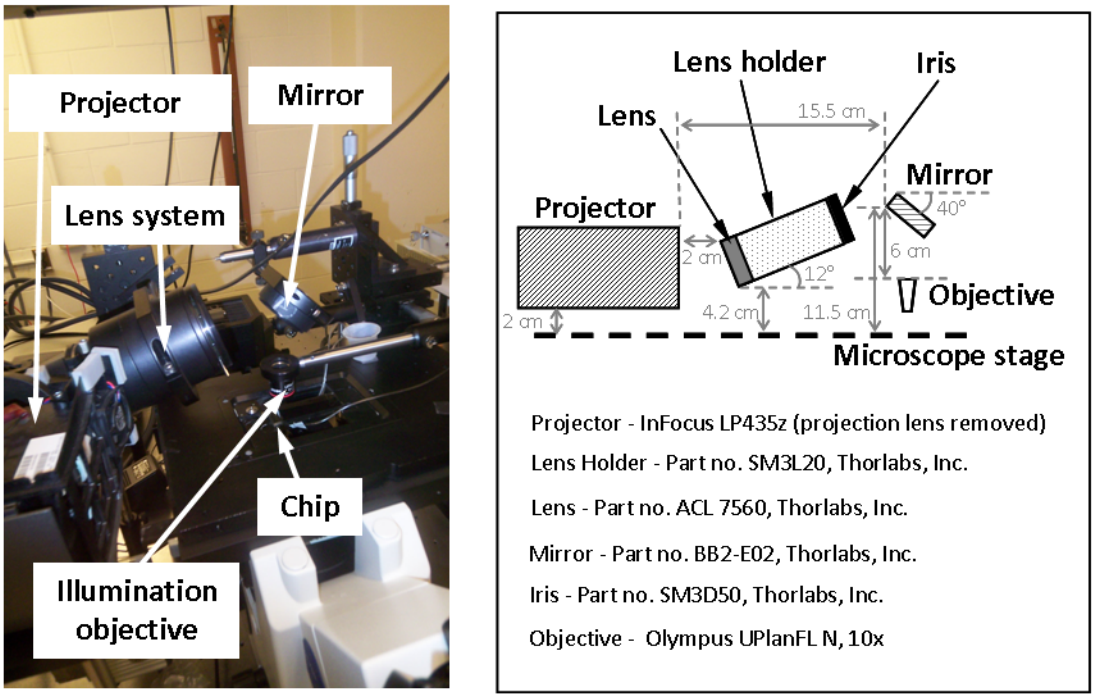

Supplementary Figure S1. Experimental setup. Left side image shows the experimental set up. The microfluidic chip is placed upside down on the microscope, illuminated from above with light from the projector and imaged from below with another objective and a camera. Flow is driven through the chip using a syringe pump. Right side image shows details of the optical components used and their spatial alignment.

This journal is © The Royal Society of Chemistry 2011

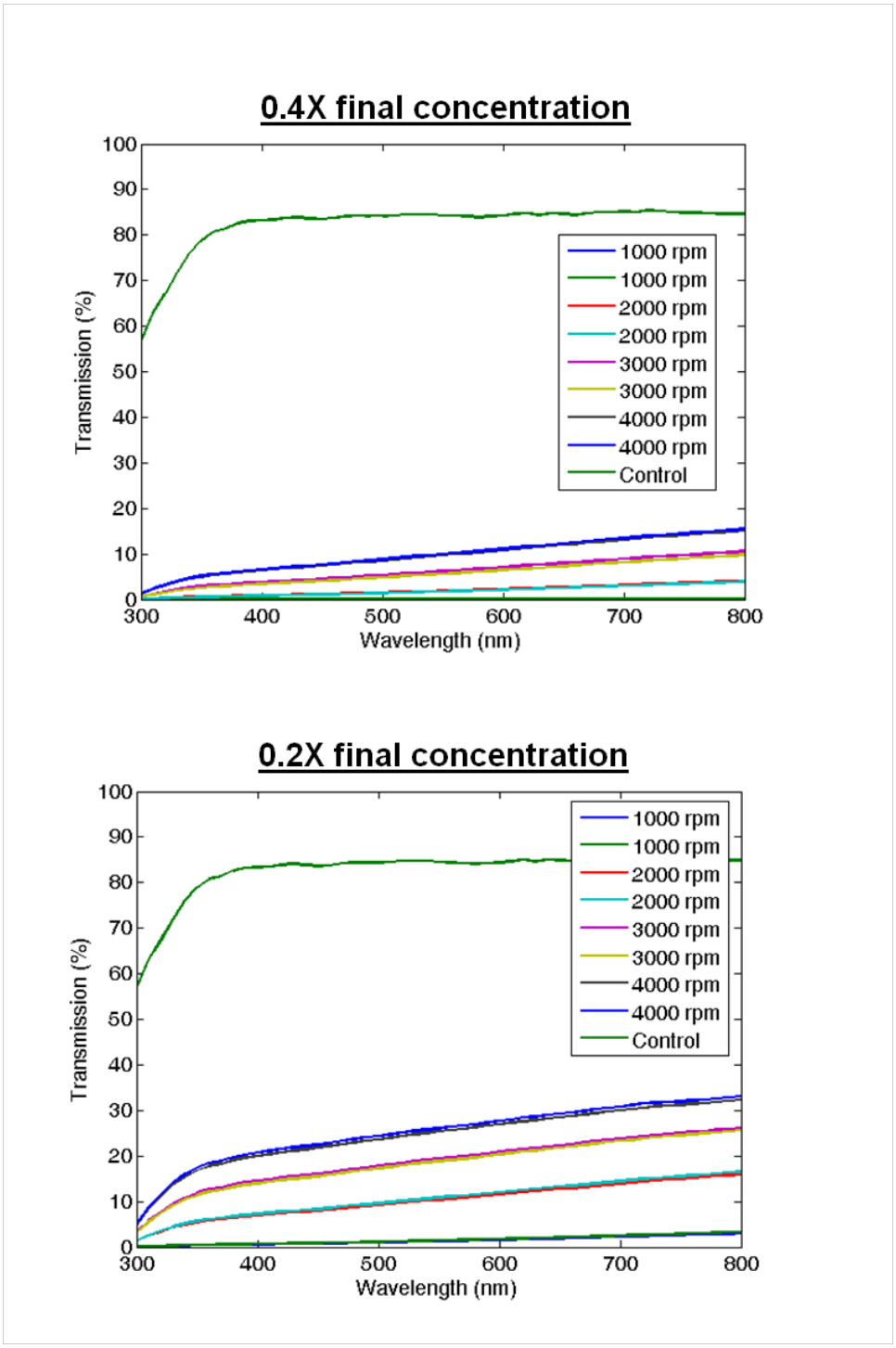

Supplementary Figure S2. Characterization of photothermal absorption layer, with wavelength. Transmission through the layer is plotted as a function of wavelength for different spin speeds.

This journal is © The Royal Society of Chemistry 2011

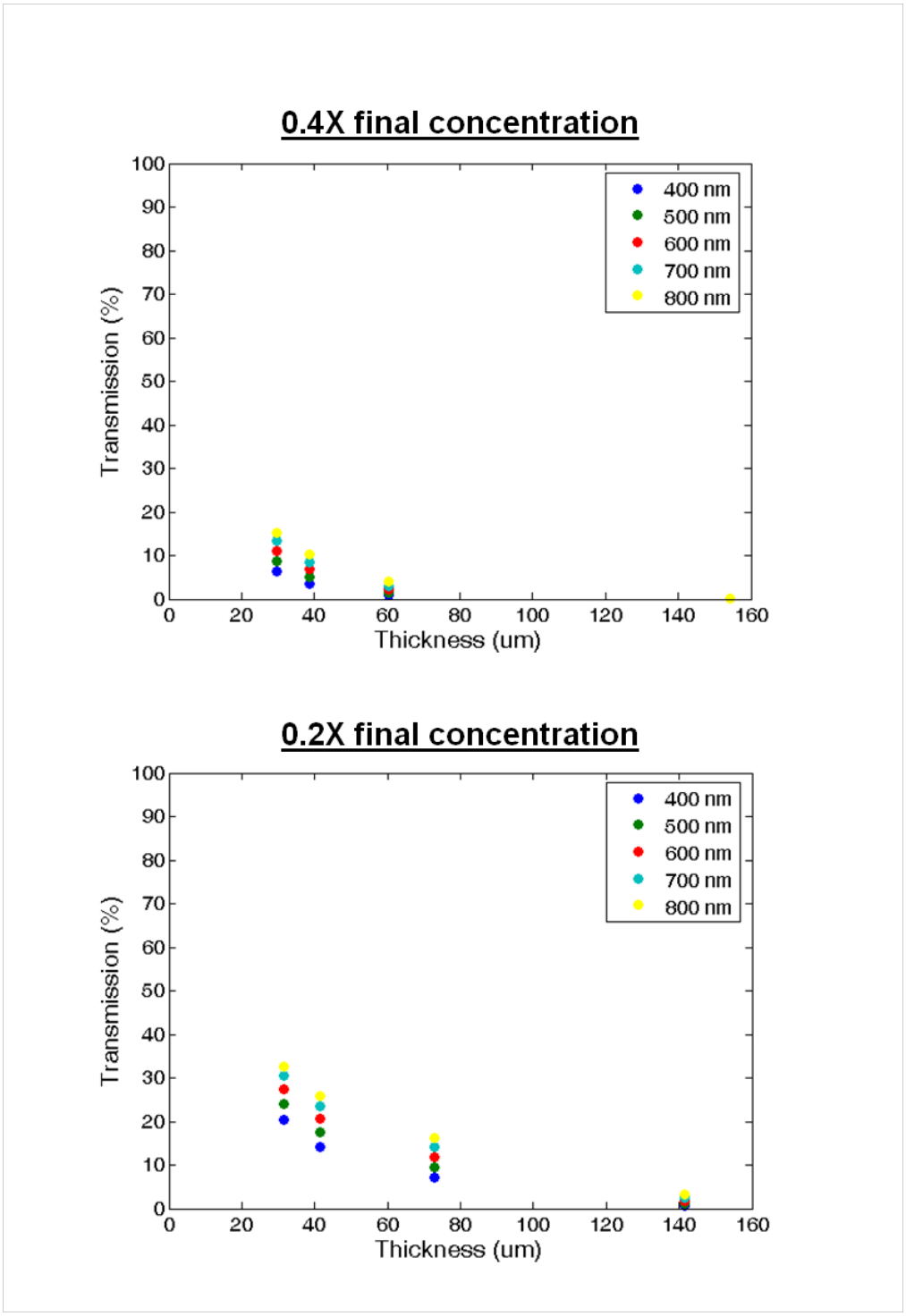

Supplementary Figure S3. Characterization of photothermal absorption layer, with absorber thickness. Transmission through the layer is plotted as a function of absorber thickness for different wavelengths.

This journal is © The Royal Society of Chemistry 2011

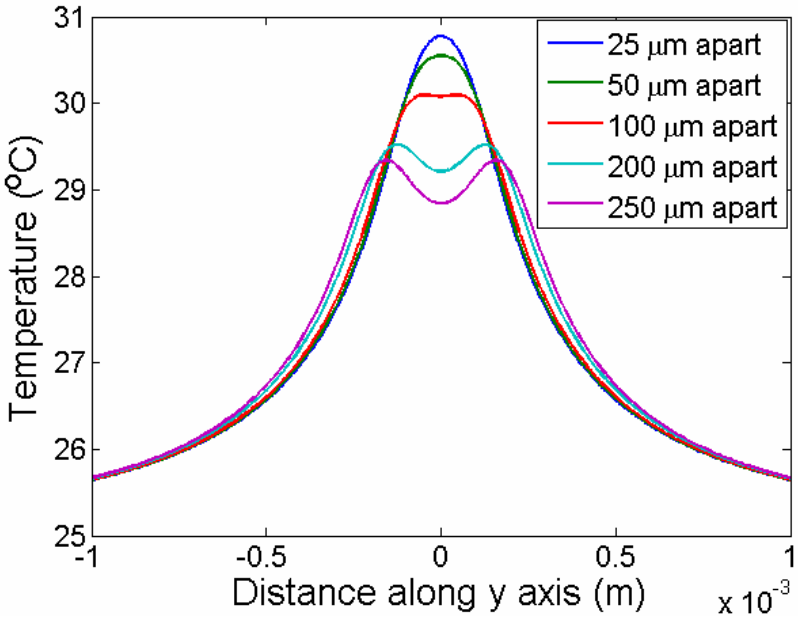

Supplementary Figure S4. Numerical characterization of spatial resolution. Temperature profile is plotted for two identical heat sources, on varying the spacing between the sources.

This journal is © The Royal Society of Chemistry 2011

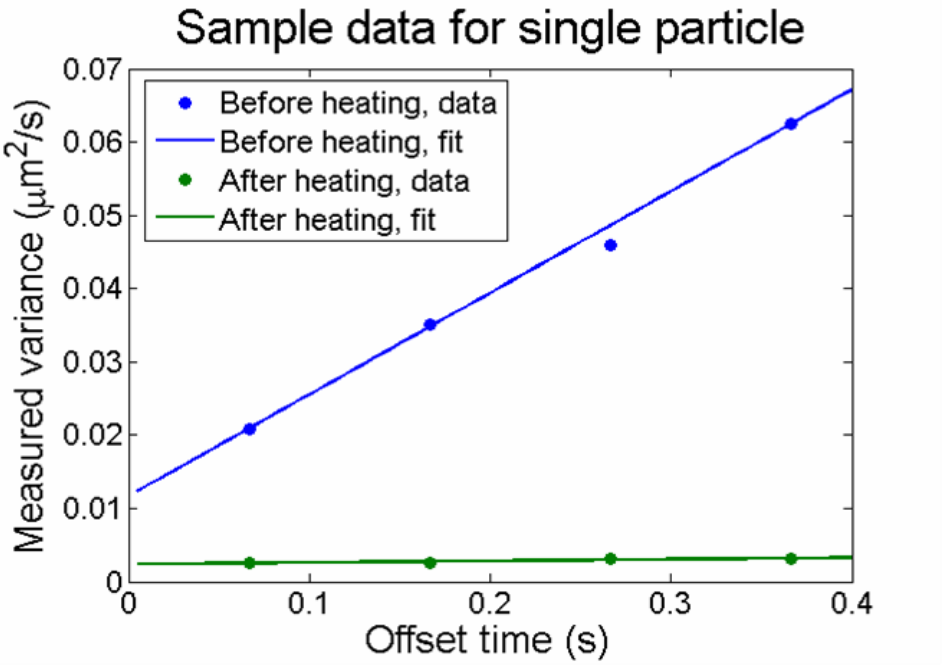

Supplementary Figure S5. Net variance of position vs. time for 210 nm polystyrene bead before and after heating. The slope of the line before heating is 0.139 $\mu m^2/s$ and after is 0.002 $\mu m^2/s$, corresponding to diffusivities of 0.069 $\mu m^2/s$ and 0.001 $\mu m^2/s$ respectively (See Supplementary Discussion Section 4 for details).

Electronic Supplementary Material (ESI) for Lab on a Chip
This journal is © The Royal Society of Chemistry 2011

Supplementary Discussion

Section S1. Photothermal absorption layer

The substrate used in our experiments consists of a glass slide covered with a thin layer of PDMS, followed by an absorbing layer. 60g of PDMS (50g of PDMS A mixed with 10g of PDMS B) was poured onto three glass slides placed in a petri dish and allowed to cure on a flat surface at room temperature overnight. The dish was then placed in a convection oven set at 80 ºC for 2 hours. This process ensured that the PDMS layer on the glass slide was flat. The reason for using a PDMS rather than glass substrate is to ensure that heat is better contained within the microfluidic chamber since the thermal conductivity of PDMS is less than that of glass (0.18 $Wm^{-1}K^{-1}$ for PDMS as opposed to 1.4 $Wm^{-1}K^{-1}$ for glass [1]). An absorbing layer was then created on top of this PDMS/glass substrate using a mixture of carbon black, PDMS A and PDMS B in the ratio 0.01:1:0.05 by weight. The process of preparing the absorbing layer was as follows. First, PDMS A and carbon black were mixed together and the mixture was sonicated for 2 hours. PDMS B was then added to the above mixture and this was dessicated for 20 minutes, followed by sonication for 30 minutes. The carbon black and PDMS mixture was then immediately spun on the PDMS/glass substrate to prevent the mixture from curing. The spinning was done at 1400 rpm with a ramp of 336 rpm/s. We also investigated the effect of varying spin speed on the thickness and transmission characteristics of the substrate as described below. After spinning, the substrate was once again dessicated for 30 minutes and then baked in a convection oven at 80 ºC for 2 hours.

This journal is © The Royal Society of Chemistry 2011

We characterized the photothermal absorption layer by doing transmission measurements using an optical spectrophotometer. We carried out measurements at different concentrations of carbon black, though we were unable to carry out these measurements at the concentration eventually used for experiments since the transmission through those substrates was too low to be detected by the spectrophotometer. We present results here for films having 0.4 times (0.4X) and 0.2 times (0.2X) the carbon black concentrations used in our final experiments. We prepared films on plain glass substrates at spin speeds in the range of 1000 – 4000 rpm, and measured both the thickness and the transmission of the films. The results are shown in Supplementary Figures S2 and S3. The control here refers to measurements taken with no absorbing film. Two sets of measurements were carried out for each spin speed as indicated in Supplementary Figure S2. It is clear through this data that transmission through the absorption layer can be modulated through two variables (a) the concentration of absorber or carbon black used and (b) the thickness of the absorption layer. We used fluidic modeling, and experimental trials to finally pick the concentration and thickness of carbon black used in the results discussed above. We found that spin speeds in the range of 1200 rpm – 1400 rpm, and a carbon black to PDMS A to PDMS B ratio of 0.01:1:0.05 gave us the best heating results, with just enough heat being input to the system to cause gelation but not too much heat to unduly gel the entire fluidic chamber.

This journal is © The Royal Society of Chemistry 2011

Section S2. Thermally Induced Secondary Flows

Various thermally induced secondary flow phenomenon can exist that could have the potential to affect the flow profile in our system. Here, we will discuss the effect of thermocapillary flows, buoyancy driven flows and viscosity driven flows.

The effect of temperature gradients could result in surface tension gradients, which have previously been demonstrated to actuate flow of bubbles in microfluidic devices [2]. This thermocapillary effect however requires the presence of a fluid-fluid interface. Although such an interface does occur initially between the pluronic solution and air while our microfluidic device is being filled, it does not subsequently exist during device operation. Thus, we do not expect to see thermocapillary driven flows here.

Buoyancy driven flows occur as a result of a density gradient created as a consequence of a thermal gradient. Such a density gradient must exist opposite to the direction of gravity, thus driving hot fluid from the bottom of the chip to the top, and cold fluid from the top to the bottom. However, as we see from Figure 2a, the temperature profile is fairly uniform along the z axis. The relative effect of buoyancy and viscosity driven flows can be examined through the use of the Grashof number, Gr [3] given by $Gr = g\alpha(\Delta T)h^3/\nu^2$, where α is the thermal expansion coefficient, h is the height of the chip, g is acceleration due to gravity, ΔT is the temperature difference and ν is kinematic viscosity. For $Gr << 1$, we expect viscous effects to dominate over buoyancy effects and thus we can neglect buoyancy driven thermal flows. Here, for $\alpha = 3.3 \times 10^{-4}$ /K, h = 50 µm, ΔT =

This journal is © The Royal Society of Chemistry 2011

5K and $\nu = 10^{-6}$ m^2/s (using values for water), we find that Gr = 0.002. Since Gr << 1, we do not expect buoyancy driven flows to significantly impact our system.

Viscosity driven flows have been demonstrated by the rapid motion of a thermal hot spot within a microfluidic device [4]. Here, the thermal gradient results in a corresponding viscosity gradient in the device, to generate flow in a direction opposite to that of the movement of the spot. However, these researchers were only able to generate flows while moving the spot at a frequency of 5 kHz. Since we do not cycle the hot spot in our system, and in fact only move the images slowly at brief intervals, if at all, we do not expect thermally induced viscosity driven flows to occur here.

This journal is © The Royal Society of Chemistry 2011

Section S3. Fluid dynamic modeling

Fluidic simulations were carried out using COMSOL. Since the thermal Peclet number characterizing our system is low, we expect diffusion to dominate over convection in the heat transfer. The Peclet number, *Pe* is defined as $Pe = Ul/\alpha$, where U is the characteristic velocity, l the characteristic length and α the thermal diffusivity. Typical values for our system are U = 500 μm/s, l = 50 μm (channel height) and $\alpha = 1.4 \times 10^{-7}$ m^2/s, thus $Pe = 0.18$. We therefore modeled only the diffusion equation while solving the heat transfer problem. The equation we solved for was

$$\nabla \cdot (k \nabla T) = 0 \qquad (1)$$

where k is the thermal conductivity and T is the temperature. While analyzing the effects of the thickness and absorbance of the photothermal absorption layer as discussed below, we solved a modified version of the above equation for the domain containing the absorption layer, to include a volumetric heat source term q such that

$$\nabla \cdot (k \nabla T) + q = 0 \qquad (2)$$

Photothermal absorption layer

We have carried out fluidic simulations using COMSOL in order to investigate the effect of substrate thickness and substrate absorption characteristics on the temperature rise in the fluid in a microfluidic chamber. From the Beer-Lambert law, for light of intensity I_0 incident on an absorbing layer of thickness x, having an absorption coefficient α, the transmitted light intensity, I (assuming no reflection from the surface) is given by

$$I = I_0 e^{-\alpha x} \qquad (3)$$

while the volumetric heat flux generated through the absorber, q is given by

This journal is © The Royal Society of Chemistry 2011

$$q = -\frac{dI}{dx} = \alpha I_0 e^{-\alpha x} \qquad (4)$$

We modeled the heat transfer due to this volumetric heating for photothermal absorption layers of different thickness and having different absorption characteristics. Based on the transmission measurements carried described in Section S1, we considered absorber layers having absorption coefficients, α of 0.04 μm^{-1}, 0.07 μm^{-1} and 0.18 μm^{-1}. For each of these values of absorption coefficients, we carried out simulations for substrates having thickness varying from 25 - 200 µm. The microfluidic chip used for the simulations is shown in Figure 2a where the simulated region is half the actual chip since the temperature profile is symmetric across the x axis. The microfluidic chamber modeled in these simulations had dimensions 1mm X 1mm X 50 µm. The region of heating was a rectangle of dimensions 100 µm X 100 µm, located at the center of the chip. Convective flux boundary conditions were applied at all the external interfaces except the plane of symmetry at which a thermal insulation boundary condition ($\nabla T \cdot n = 0$) was applied, and the bottom substrate at which a constant temperature boundary condition was applied.

Spatial Resolution

We examined the effect of placing multiple heat sources close to each other using simulations, as shown in Supplementary Figure S4. Here, we have two sources that are 100 µm X 100 µm, placed at various distances apart ranging from 25 - 250 µm. This type of illumination pattern represents a microfluidic channel created within a larger chamber, and this characterization allows us to determine the smallest size of channel that can be created. The height of the chamber here is 50 µm with a 100 µm thick absorber having

This journal is © The Royal Society of Chemistry 2011

an absorption coefficient of 0.18 μm^{-1}. This characterization was carried out to determine the nature of the temperature profile and the ability to distinguish the two separate peaks corresponding to the two sources, rather than the absolute value of the temperature itself (since that can be easily modulated by increasing the size or intensity of the source). We would expect a temperature difference of at least 1-2 °C above and below the gelation temperature between the peak temperatures at the center of the hot spots, and the region between them to sufficiently resolve gelled and ungelled regions. As this figure clearly demonstrates, there is poor resolution of the temperature profile for sources that are closer than about 250 μm. In fact, sources closer than 100 μm appear like a single source. However, these simulations represent preliminary work on characterizing this spatial resolution, and better understanding of the temperature profiles of individual sources and their interaction is needed to understand and improve the limits of this resolution.

This journal is © The Royal Society of Chemistry 2011

Section S4. Calculation of diffusion coefficients

Trajectory data similar to that shown in Figure 5c was used to calculate the diffusion coefficients of the polystyrene beads before and after heating. Trajectory data was obtained using the Video Spot Tracker software developed by the Computer Integrated Systems for Microscopy and Manipulation (CISMM) at UNC Chapel Hill (for tracking particle motion), or the ParticleTracker plugin for ImageJ (for tracking DNA motion). The former involves the use of the "cone kernel" for tracking particles, useful for tracking spots that are brighter in the center and the drop off to dim regions and involve a weighted average approach, with a weight of 1 at the center and 0 at the specified radius [5]. The latter algorithm works using a feature point detection system that finds local intensity maxima [6]. We used a relation described in [7] that helps account for the error in measuring particle variance due to limitations on the spatial and temporal resolution of the system. The details of this analysis are not presented here and the readers are referred to [7] for further reference. The trajectory data indicates the (x, y) position of a particle as a function of time. With this data, it was possible to extract incremental displacements, ($\Delta x(t)$, $\Delta y(t)$) of particles at 4 different time intervals t of 0.1 - 0.4s. This was done by measuring the displacement of the particle from an initial position through the desired time interval, for multiple initial positions through the particle trajectory, to create a distribution of particle displacements. As described in [7], the variance of the measured displacement in the x direction or Δx, given by $Var(\Delta x)$ is then given by the relation,

$$Var(\Delta x) = 2D(t - \sigma/3) + 2\varepsilon^2 \qquad (5)$$

This journal is © The Royal Society of Chemistry 2011

where σ indicates the exposure time of the measurement, ε denotes the spatial resolution of the system and D denotes the diffusion coefficient. The exposure time for our measurements was 0.1 s. We combined the data along the x and y axis to get a better estimate for D, using the relation

$$\left(Var\left(\Delta x\right)+Var\left(\Delta y\right)\right)/2 = 2D\left(t-\sigma/3\right)+2\varepsilon^2 \qquad (6)$$

The variances were calculated from the measured displacement data for different time intervals as discussed above and plotted against (t – σ/3). A sample data set is shown in Supplementary Figure S5 for a particle before and after heating. The Matlab curve fitting tool box was then used to obtain a linear fit to such data for 10 different particles. The slope of the curve in each case is equal to twice the diffusion coefficient as seen from Equation 6. This technique thus does not have a theoretical lower limit in terms of resolution; however there is likelihood of error in prediction of diffusivity using their algorithm since it requires a linear fit to be applied to the data. These researchers have reported an error of ~ 10% while using their technique.

This journal is © The Royal Society of Chemistry 2011

References

[1] Erickson, D., Sinton, D. & Li, D. Q. Joule heating and heat transfer in poly(dimethylsiloxane) microfluidic systems. *Lab Chip* **3**, 141-149 (2003).

[2] Ohta, A. T., Jamshidi, A., Valley, J. K., Hsu, H. Y. & Wu, M. C. Optically actuated thermocapillary movement of gas bubbles on an absorbing substrate. *Appl. Phys. Lett.* **91**, 074103 (2007).

[3] Incropera, F. P. & DeWitt, D. P., in Heat and Mass Transfer (John Wiley & Sons, 2002), pp. 355.

[4] Weinert, F. M. & Braun, D. Optically driven fluid flow along arbitrary microscale patterns using thermoviscous expansion. *Journ. of Appl. Phys.* **104**, 104701 (2008).

[5] http://cismm.cs.unc.edu/resources/software-manuals/video-spot-tracker-manual/

[6] Sbalzarini, F. and Koumoutsakos, P. Feature Point Tracking and Trajectory Analysis for Video Imaging in Cell Biology. *Journ. of Struct. Bio.* **151**, 182-195 (2005).

[7] Savin, T. and Doyle, P. S. Static and Dynamic Errors in Particle Tracking Microrheology. *Biophys. Journ.* **88,** 623-638 (2005).